JBC RESEARCH ARTICLE

Structural features of *Cryptococcus neoformans* bifunctional GAR/AIR synthetase may present novel antifungal drug targets

Received for publication, March 12, 2021, and in revised form, August 6, 2021 Published, Papers in Press, August 17, 2021,
https://doi.org/10.1016/j.jbc.2021.101091

Sheena M. H. Chua[1,2], Maha S. I. Wizrah[1,2], Zhenyao Luo[2,3], Bryan Y. J. Lim[1,2,3], Ulrike Kappler[1,2], Bostjan Kobe[1,2,3], and James A. Fraser[1,2,*]

From the [1]Australian Infectious Diseases Research Centre, [2]School of Chemistry & Molecular Biosciences, and [3]Institute for Molecular Bioscience, The University of Queensland, St Lucia, Queensland, Australia

Edited by Joseph Jez

***Cryptococcus neoformans* is a fungus that causes life-threatening systemic mycoses. During infection of the human host, this pathogen experiences a major change in the availability of purines; the fungus can scavenge the abundant purines in its environmental niche of pigeon excrement, but must employ *de novo* biosynthesis in the purine-poor human CNS. Eleven sequential enzymatic steps are required to form the first purine base, IMP, an intermediate in the formation of ATP and GTP. Over the course of evolution, several gene fusion events led to the formation of multifunctional purine biosynthetic enzymes in most organisms, particularly the higher eukaryotes. In *C. neoformans*, phosphoribosyl-glycinamide synthetase (GARs) and phosphoribosyl-aminoimidazole synthetase (AIRs) are fused into a bifunctional enzyme, while the human ortholog is a trifunctional enzyme that also includes GAR transformylase. Here we functionally, biochemically, and structurally characterized *C. neoformans* GARs and AIRs to identify drug targetable features. GARs/AIRs are essential for *de novo* purine production and virulence in a murine inhalation infection model. Characterization of GARs enzymatic functional parameters showed that *C. neoformans* GARs/AIRs have lower affinity for substrates glycine and PRA compared with the trifunctional metazoan enzyme. The crystal structure of *C. neoformans* GARs revealed differences in the glycine- and ATP-binding sites compared with the *Homo sapiens* enzyme, while the crystal structure of AIRs shows high structural similarity compared with its *H. sapiens* ortholog as a monomer but differences as a dimer. The alterations in functional and structural characteristics between fungal and human enzymes could potentially be exploited for antifungal development.**

Purines are key biological molecules involved in a plethora of roles including energy metabolism, cell signalling, and encoding the genome for all organisms. To survive, an organism must either salvage purines from the environment *via* a family of dedicated phosphoribosyltransferases or synthesize purines through the highly conserved enzymes of the *de novo* biosynthesis pathway. Historically, the purine metabolic pathway has revealed bountiful targets for drug development. Several important drugs that act by inhibiting specific enzymes in the pathway are routinely used to this day; these include acyclovir for treating viral infections, allopurinol for treating gout, and azathioprine for preventing organ transplant rejection (1–3). Among the drugs that have been developed by targeting purine biosynthesis, antimicrobials that act specifically against bacterial or fungal pathogens have yet to be discovered.

There is a limited number of effective antifungals for treatment of disseminated fungal infections caused by species such as the basidiomycete yeast *Cryptococcus neoformans* (4). Infections caused by this opportunistic fungus present mainly as meningoencephalitis, a condition commonly encountered particularly in sub-Saharan Africa due to the high prevalence of AIDS in this region (5). The gold standard treatment for meningoencephalitis is amphotericin B, flucytosine, and fluconazole. These treatments have not changed significantly for decades despite high toxicity, excessive cost, limited effectiveness, as well as their association with drug resistance and cross-reactivity (6–10).

The enzymes of the *de novo* purine biosynthesis pathway are a potential drug target for antifungals against *C. neoformans* as the environmental niche of the fungus, purine-rich bird guano, is a stark contrast to the purine-poor human central nervous system it infects (11, 12). Consistent with this, previous research has revealed that successful infection in a murine model requires multiple enzymes that catalyze the conversion of inosine monophosphate (IMP) to adenosine triphosphate (ATP) and guanosine triphosphate (GTP), the final steps of *de novo* purine biosynthesis (13–15).

De novo biosynthesis of the purine base is comprised of two major components: the five-step synthesis of an imidazole ring, followed by a six-step process to form the second ring, pyrimidine, to create the first heterocyclic purine base, IMP. *De novo* biosynthesis of the first part of this structure begins with phosphoribosyl-pyrophosphate (PRPP) amidotransferase ($PRPP_A$, EC 2.4.2.14), which hydrolyzes l-glutamine and transfers the liberated amine group to PRPP,

* For correspondence: James A. Fraser, j.fraser1@uq.edu.au.

creating phosphoribosyl-amine (PRA; Fig. 1*A*) (16). The second enzyme, phosphoribosyl-glycinamide (GAR) synthetase (GARs, EC 6.3.4.13), catalyzes the ATP-dependent ligation of l-glycine to PRA, *via* a phosphorylated intermediate, to yield GAR (17). GAR transformylase (N^{10}-fTHF-GAR$_T$, EC 2.1.2.2) performs the third step that ligates the formyl group from 10-formyltetrahydrofolate (N^{10}-fTHF) to GAR, producing phosphoribosyl-formylglycinamide (FGAR) (18). The fourth enzyme, phosphoribosyl-formylglycinamidine (FGAM) synthetase (FGAMs, EC 6.3.5.3), activates the FGAR amide oxygen in the ATPase domain to produce an iminophosphate intermediate, which is amidated by ammonia, channelled *via* a structural domain from the glutaminase domain to create FGAM (19). Finally, phosphoribosyl-aminoimidazole (AIR) synthetase (AIRs, EC 6.3.3.1) catalyzes the ATP-dependent activation of the FGAM formyl oxygen, which reacts with a nearby nitrogen to close the imidazole ring of the unfinished purine base and forms AIR (20).

While these first five enzymes in *de novo* purine biosynthesis mostly exist as monofunctional proteins in the Archaea and Bacteria, in many Eukaryotes the genes encoding these enzymes have fused to encode multifunctional proteins consisting of up to three components of the pathway in a single open reading frame (21). One of these multifunctional proteins consists of GARs, responsible for the second step of the pathway, fused at its C terminus to AIRs, which performs the fifth step. The bifunctional enzyme is found in the Amoebozoa and Fungi. In the Metazoa, this fusion protein has expanded to include GAR$_T$, mediating the third step of *de novo* purine biosynthesis, forming a trifunctional enzyme (TrifGART). Crystal structures have been determined for unfused bacterial GARs and AIRs from *Escherichia coli, Geobacillus kaustophilus*, and *Thermus thermophiles* (17, 22–25). *Homo sapiens* is the only eukaryote with crystal structures determined for single unit GARs, AIRs, and GAR$_T$. The missing piece to this picture is the structure of the fungal bifunctional GARs/AIRs, which represents an intermediate state between the single unit enzymes of the Bacteria and triple unit fusion of the Metazoa. This major difference may potentially be exploited in the development of new, fungal enzyme-specific purine biosynthesis inhibitors to treat disseminated life-threatening mycoses.

Here we present the characterization of the bifunctional GARs/AIRs from *C. neoformans*. We have shown that this enzyme is critical for virulence in a murine infection model and have identified differences in enzyme substrate specificity compared with metazoan species. We have also determined *C. neoformans* X-ray crystal structures of the GARs and AIRs units that revealed potentially exploitable differences in the GARs glycine- and ATP-binding sites when compared with the human ortholog.

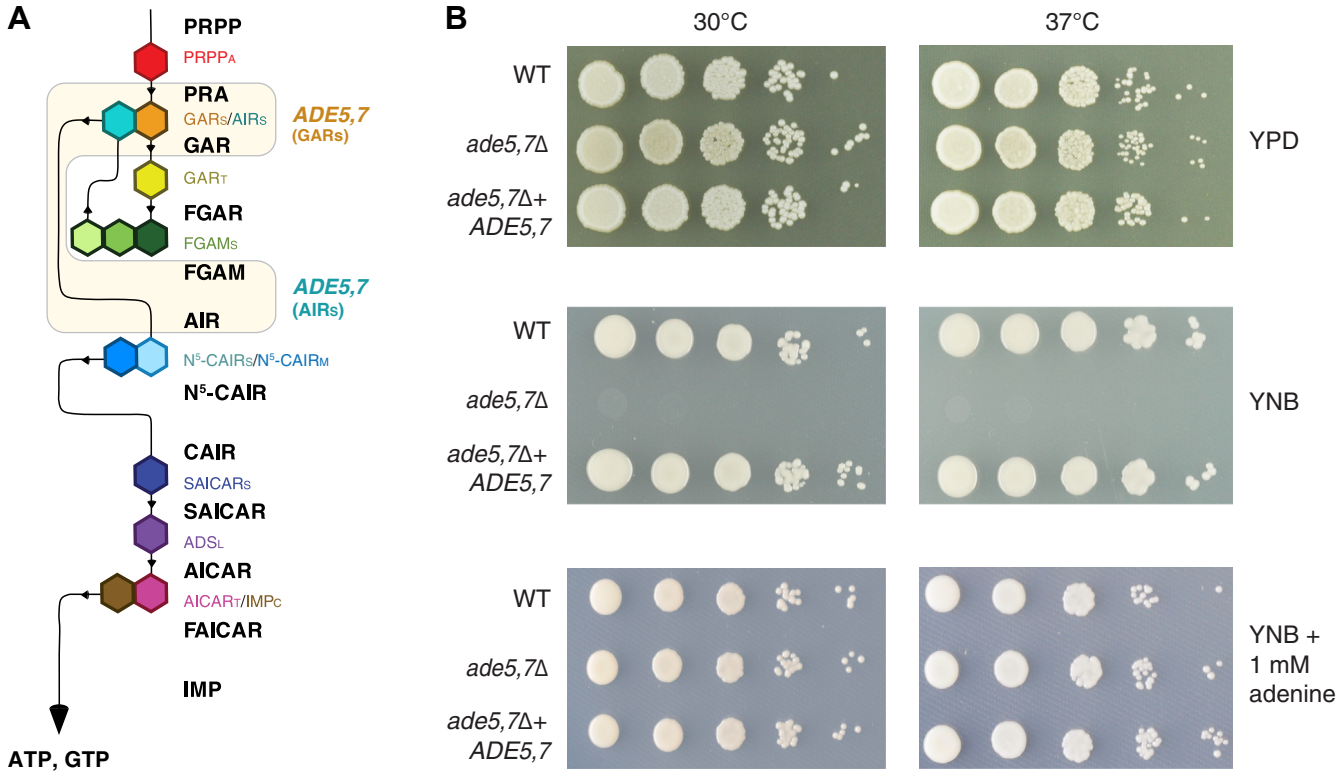

Figure 1. *Cryptococcus neoformans ade5,7*Δ mutants are adenine auxotrophs. *A*, *de novo* purine biosynthesis pathway. Bifunctional GARs/AIRs are encoded by *ADE5,7* in *C. neoformans*. Purine biosynthesis enzymes are represented as coloured hexagons. Enzyme fusions are represented by hexagons joined together. *B*, growth phenotypes of wild-type, *ade5,7*Δ, and *ade5,7*Δ+*ADE5,7* strains. Strains were serially tenfold diluted and 5 μl of each dilution spotted on YPD, YNB, and YNB supplemented with 1 mM adenine, then grown at 30 and 37 °C. Pictures were taken after 48 h of growth. The *ade5,7*Δ strain shows no growth on YNB agar without supplementation with adenine.

Results

Identification of the gene encoding GARs and AIRs in C. neoformans

To identify GARs and AIRs in *C. neoformans*, a reciprocal best hit BLAST analysis was performed to identify the homolog of *S. cerevisiae* Ade5,7 in the H99O-type strain genome. Consistent with our previous observations that these enzymes appeared to be fused in all fungi, querying the *C. neoformans* genome with the *S. cerevisiae* protein identified a single locus, *CNAG_06,314*. The predicted protein sequence translated from *CNAG_06314* was used in a BLASTp search against the *S. cerevisiae* genome and returned *ADE5,7* as the single hit. As with other *C. neoformans* genes, we named *CNAG_06314 ADE5,7,* based on the *S. cerevisiae* nomenclature.

A protein alignment of *S. cerevisiae* and *C. neoformans* Ade5,7 revealed 52.1% identity, indicating a moderate level of conservation. Investigating the conservation of the individual GARs and AIRs functional units of the fusion protein showed conservation was not restricted to a single domain, with 50.1% and 52.6% identity, respectively. By comparison, the *C. neoformans* bifunctional Ade5,7 protein alignment with the equivalent enzymatic units of *H. sapiens* TrifGART yields an identity of 42.8% for GARs and 45.4% for AIRs.

C. neoformans ade5,7*Δ mutants are adenine auxotrophs*

To determine whether the *ADE5,7* gene is essential for *de novo* purine production, an *ADE5,7* gene deletion construct was created and introduced *via* biolistic transformation-mediated homologous recombination into the *C. neoformans* H99O-type strain genome. Transformants were analyzed by Southern blot to identify and validate deletion mutants. The *ade5,7Δ* strain could grow when exogenous adenine was supplemented in the yeast nitrogen base (YNB) media, but not without; it is an adenine auxotroph as expected (Fig. 1*B*). On nutrient-rich YPD media, the *ade5,7Δ* mutant could also grow, but the colonies were smaller compared with the wild-type strain at both 30 °C and human body temperature. This poor growth could be resolved by the addition of exogenous adenine. Reintroducing the wild-type *ADE5,7* gene by inserting it into the Safe Haven locus on chromosome 1 (26) to create the *ade5,7Δ+ADE5,7* strain produced wild-type characteristics on all media, verifying that the observed phenotypes were due to the loss of *ADE5,7*.

Deletion of ADE5,7 *in* C. neoformans *does not affect production of major virulence traits*

After confirming the *ade5,7Δ* adenine auxotrophic phenotype, the deletion and complemented strains were tested for the production of the major virulence traits of *C. neoformans*. Virulence trait production was measured by spotting the strains on BSA agar to test for protease, l-3,4-dihydroxyphenylalanine (L-DOPA) agar for melanin, egg yolk agar for phospholipase B, and Christensen's urea agar for urease. Another virulence trait, capsule formation, was visualized under the microscope using India ink following growth in RPMI 1640 medium.

There was no detectable difference in the production of protease, melanin, phospholipase B, urease, and capsule by the *ade5,7Δ* mutant compared with the wild-type or complemented strains (Fig. S1). The results indicate that unlike a number of other purine enzyme deletion mutants in *C. neoformans* that have been studied previously, the loss of the bifunctional GARs/AIRs enzyme did not have a visible effect on virulence trait production (13–15).

ADE5,7 *is essential for* C. neoformans *virulence in a murine inhalation infection model*

The GARs/AIRs deletion strain was employed in a murine inhalation infection model to determine whether the loss of the gene encoding this bifunctional enzyme has an impact on the virulence of *C. neoformans in vivo*. As the availability of purines in the mouse CNS is comparable to the purine-poor human CNS environment (27), it was predicted that the deletion of *ADE5,7* would cause a loss of virulence.

Groups of ten mice were infected with either the wild-type, the deletion mutant, or the complemented strain. Mice were monitored daily after infection and were euthanized based on either the symptoms of meningoencephalitis or a 20% loss of body weight; the spleen, kidney, liver, lungs, and brains from all euthanized mice were collected, homogenized, and plated on YNB media supplemented with adenine to quantitate fungal burden.

All mice infected with the wild-type and complemented *ade5,7Δ+ADE5,7* strains succumbed to illness within 3 weeks. In stark contrast, all mice infected with the *ade5,7Δ* mutant survived and appeared healthy at the end of the experiment; the mutant is avirulent (Fig. 2*A*). Consistent with this result, while the fungal burden load for all organs was equivalent in mice infected with the wild-type and *ade5,7Δ+ADE5,7* strains (p-value > 0.05), the mice infected with the *ade5,7Δ* mutant had no fungal burden detected in their homogenized organs (Fig. 2*B*). These results demonstrate that *ADE5,7* is essential for *C. neoformans* during the infection process, highlighting its potential as an antifungal target.

Oligomeric states of C. neoformans *bifunctional GARs/AIRs and its single enzymatic units*

Because GARs/AIRs are essential for *C. neoformans* virulence, the bifunctional GARs/AIRs and its functional units (GARs and AIRs) were structurally and biochemically characterized to identify differences between the fungal and human proteins that may be employable in the future for antifungal design. Recombinant His-tagged *C. neoformans* bifunctional GARs/AIRs, and the GARs and AIRs units alone, were expressed in *E. coli* and purified using immobilized metal affinity chromatography (IMAC) and size-exclusion chromatography (SEC). The predicted sizes of purified bifunctional GARs/AIRs (80 kDa), GARs (50 kDa), and AIRs (40 kDa) were confirmed by SDS-PAGE (Fig. 3, *A1–A3*, respectively).

The bifunctional enzyme and its single enzymatic units were each characterized using mass photometry to determine the oligomeric state of the proteins in solution. *E. coli* GARs was

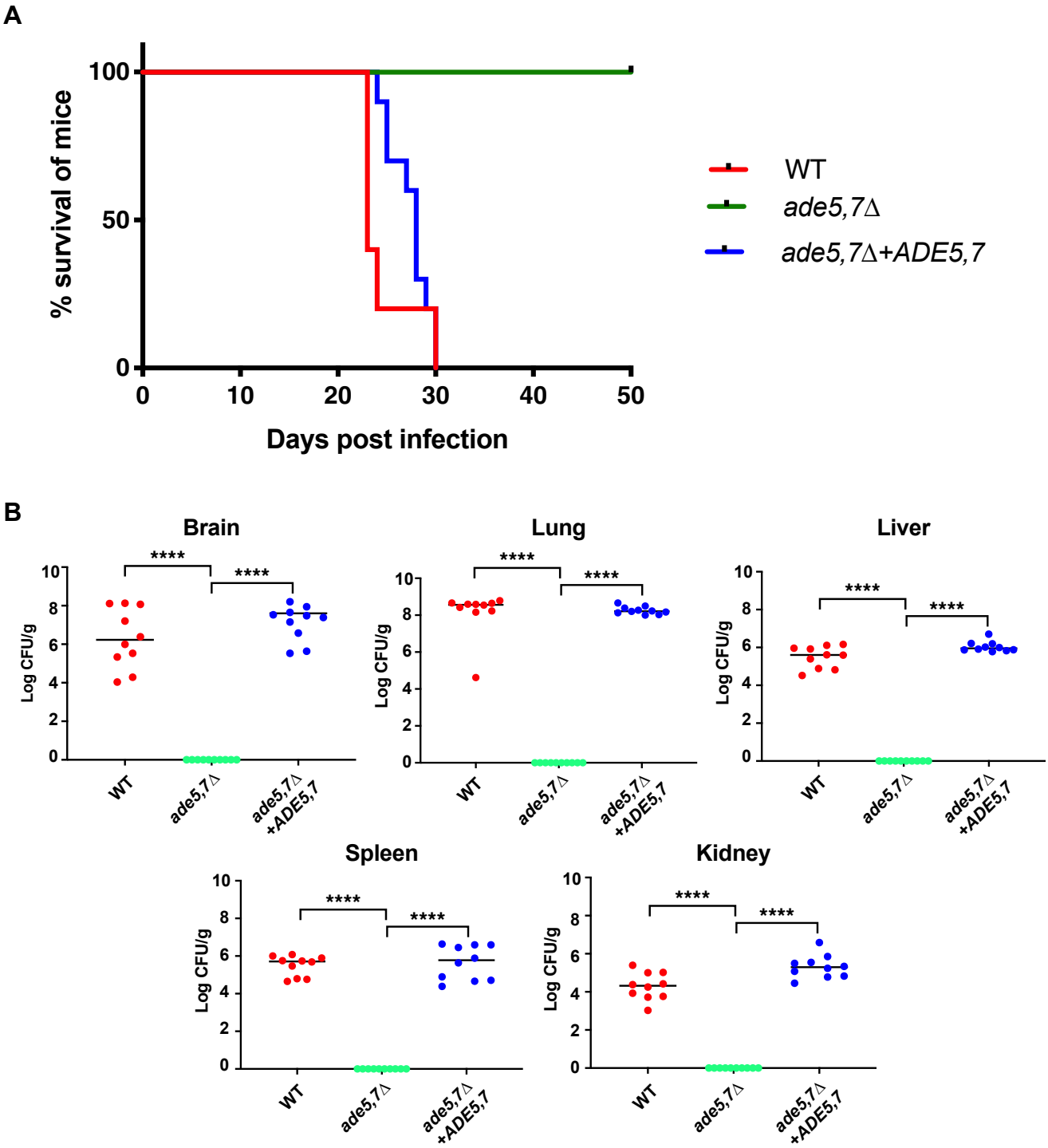

Figure 2. *ADE5,7* is essential for *Cryptococcus neoformans* virulence in a murine inhalation infection model. *A*, deletion of the gene encoding bifunctional GARs/AIRs abolishes the virulence of *C. neoformans*. Six-week-old mice were infected intranasally with 1×10^5 cells of wild-type, *ade5,7*Δ mutant, or *ade5,7*Δ*+ADE5,7* complemented strains. Kaplan–Meier survival curves are plotted and significance determined by log-rank tests. All mice infected with the *ade5,7*Δ mutant survived, and there was no significant difference between the mice survival of wild-type and *ade5,7*Δ*+ADE5,7* complemented strains (p-value > 0.05). *B*, fungal organ burden of mice infected with wild-type, *ade5,7*Δ mutant, and *ade5,7*Δ*+ADE5,7* complemented strains. Organs collected from the mice after euthanasia were homogenized and spotted on YNB plates supplemented with adenine. The fungal burden for mice infected with the wild-type and *ade5,7*Δ*+ADE5,7* was significantly higher (****p-value < 0.05) than the mice infected with the *ade5,7*Δ mutant, which did not have any fungus present.

previously shown to be a monomer by SEC with standard molecular weights, and *E. coli* AIRs to be a dimer (17, 23). Mass photometry revealed that the *C. neoformans* bifunctional GARs/AIRs consisted of ∼65% monomers (∼80 kDa) and ∼25% dimers (∼170 kDa); GARs as a single enzymatic unit were composed of ∼80% monomers (∼50 kDa) and ∼20% dimers (∼100 kDa); AIRs as a single enzymatic unit existed only as dimers (∼80 kDa) (Fig. 3, *B1–B3*, respectively). By

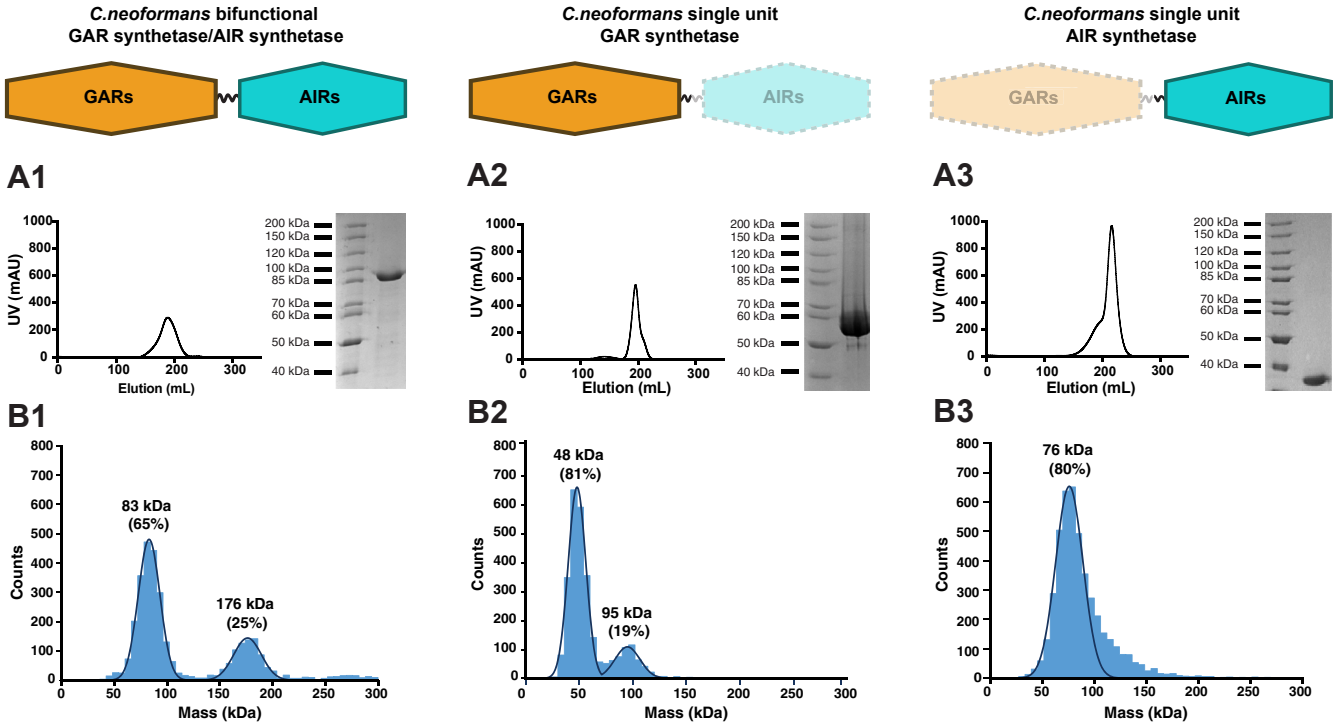

Figure 3. Oligomeric states of *Cryptococcus neoformans* bifunctional GARs/AIRs and its single enzymatic units. *A*, size-exclusion chromatography of recombinant His-tagged *C. neoformans* bifunctional GARs/AIRs and single enzymatic units (GARs and AIRs). Recombinant His-tagged *C. neoformans* protein was expressed and purified using IMAC and SEC. The predicted sizes of purified bifunctional GARs/AIRs (A1, 80 kDa), single unit GARs (A2, 50 kDa), and single unit AIRs (A3, 40 kDa) were confirmed by SDS-PAGE. *B*, oligomeric state determination of *C. neoformans* bifunctional GARs/AIRs and the single enzymatic units GARs and AIRs. Protein oligomerization in solution was determined by mass photometry, revealing monomers and dimers for bifunctional GARs/AIRs (B1), monomers and dimers for single unit GARs (B2), and dimers for single unit AIRs (B3).

comparison, small-angle X-ray scattering (SAXS) of human TrifGART previously showed the formation of dimers in solution (24). Therefore, the *C. neoformans* bifunctional GARs/AIRs have similarities to the human enzyme in terms of forming dimers, with both of the component units displaying the ability to dimerize on their own.

C. neoformans *GARs differ from characterized metazoan GARs in its substrate specificity and turnover*

We performed a biochemical characterization of bifunctional GARs/AIRs and single unit GARs to enable comparison to metazoan TrifGART (GARs/AIRs/GAR$_T$) in order to identify functional differences that may be exploitable for antifungal drug design. The recombinant proteins were characterized using steady-state enzyme kinetics of GARs activity. The substrate PRA was chemically synthesized from ribose 5-phosphate and ammonium chloride using the methodology of Schendel and colleagues (28). A coupled enzyme assay with excess molar concentrations of 8 U/ml pyruvate kinase (PK) and 10 U/ml lactate dehydrogenase (LDH) from rabbit muscle was used to measure GARs activity, where the consumption of NADH was detected spectrophotometrically at 340 nm (Fig. 4*A*).

GARs is responsible for the second enzymatic reaction in purine biosynthesis (Fig. 1*A*). Studies of the enzymes from *E. coli* and the thermophilic bacteria *Thermus thermophilus, G. kaustophilus, and Aquifex aeolicus* have shown that the GARs reaction occurs in three substeps (17, 22). First, the γ-phosphate of ATP is attacked by the oxygen from glycine, resulting in the dephosphorylation of ATP through a nucleophilic substitution. Second, glycine is phosphorylated to form a glycylphosphate intermediate. Third, the glycyl component from the carbonyl carbon of the glycylphosphate is transferred to the amine nitrogen of PRA *via* a nucleophilic acyl substitution that forms the product GAR. The enzyme specificity for the substrates participating in each of the three sub-steps was measured by varying the amounts of ATP, glycine, and PRA independently, while keeping the other substrates at a saturating concentration equivalent to ten times K_m concentrations for maximal enzyme activity.

ATP dephosphorylation for both bifunctional GARs/AIRs and single unit GARs displayed Michaelis–Menten kinetics, with very similar $K_{m\ \mathrm{app\_ATP}}$ values of 48 ± 3 μM and 52 ± 3 μM, respectively (Fig. 4*B*), and turnover numbers (k_{cat}) of 27.3 ± 0.4 s^{-1} for bifunctional GARs/AIRs and 17.3 ± 0.3 s^{-1} for the single unit GARs. As a result of the approximately twofold lower k_{cat} for the single unit GARs, k_{cat}/K_{m_ATP} for bifunctional GARs/AIRs ((5.7 ± 0.4) × 10^5 M^{-1} s^{-1}) was almost two times higher compared with single unit GARs, which had a k_{cat}/K_{m_ATP} of (3.3 ± 0.2) × 10^5 M^{-1}.

The phosphorylation of glycine also followed Michaelis–Menten kinetics with $K_{m\ \mathrm{app\_glycine}}$ values of 496 ± 20 μM for the bifunctional GARs/AIRs and 364 ± 9 μM for single unit GARs and had very similar $k_{cat}/K_{m\_glycine}$ of (5.5 ± 0.2) × 10^4 M^{-1} s^{-1} and (4.8 ± 0.1) × 10^4 M^{-1} s^{-1} (Fig. 4*B*).

Finally, Michaelis–Menten kinetics for the ligation of the glycyl component to PRA revealed a $K_{m\ \mathrm{app\_PRA}}$ of 131 ±

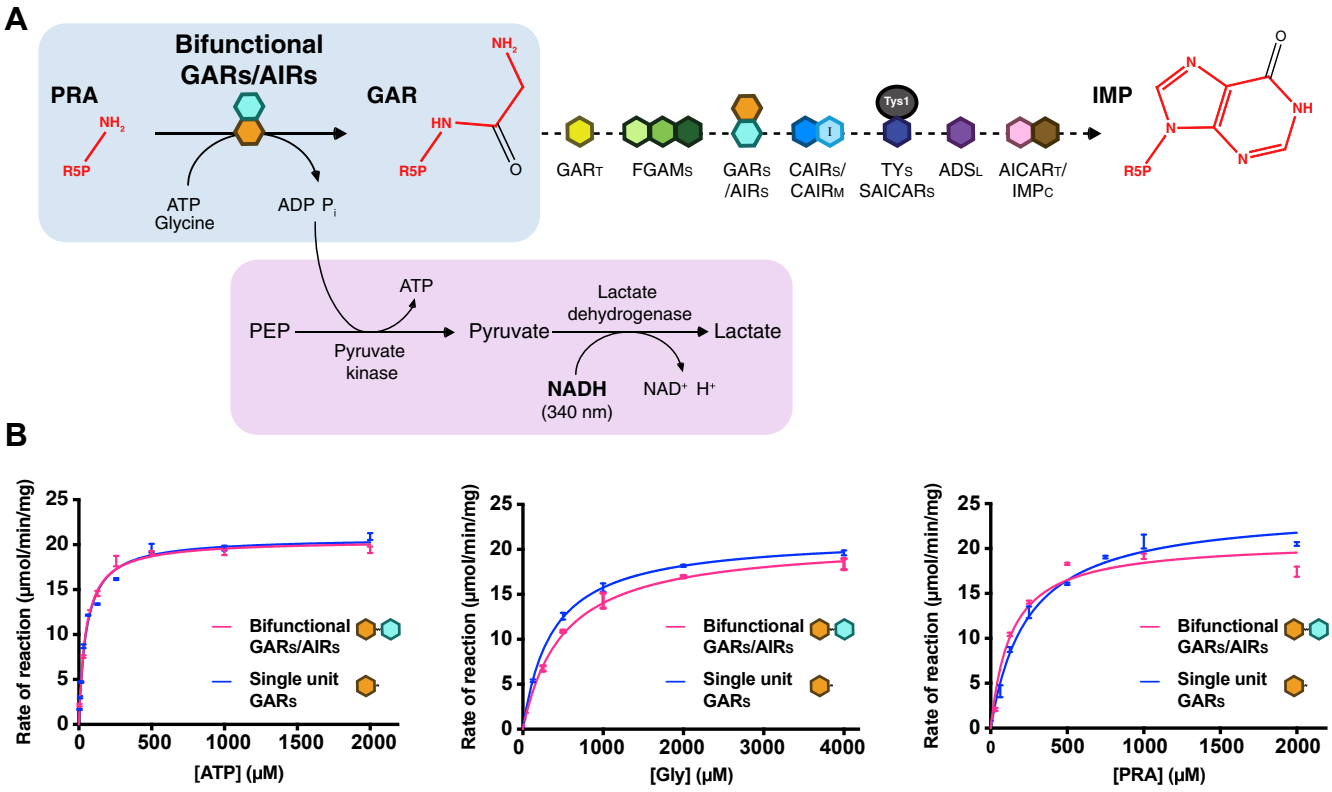

Enzyme form M.W.	Specific activity (U/mg)	k_{cat} (s^{-1})	K_m (ATP) (μM)	k_{cat} / K_m (ATP) (M^{-1} s^{-1})	K_m (Gly) (μM)	k_{cat} / K_m (Gly) (M^{-1} s^{-1})	K_m (PRA) (μM)	k_{cat} / K_m (PRA) (M^{-1} s^{-1})
Bifunctional GARs/AIRs 80 kDa	20.5 ± 0.3	27.3 ± 0.4	48 ± 3	$\left(\frac{5.7}{\pm 0.4}\right) \times 10^5$	496 ± 20	$\left(\frac{5.5}{\pm 0.2}\right) \times 10^4$	131 ± 15	$\left(\frac{2.1}{\pm 0.2}\right) \times 10^5$
Single unit GARs 50 kDa	20.8 ± 0.3	17.3 ± 0.3	52 ± 3	$\left(\frac{3.3}{\pm 0.2}\right) \times 10^5$	364 ± 9	$\left(\frac{4.8}{\pm 0.1}\right) \times 10^4$	240 ± 19	$\left(\frac{7.2}{\pm 0.6}\right) \times 10^4$

Figure 4. *Cryptococcus neoformans* GARs differ from characterized metazoan GARs in its substrate specificity and turnover. *A*, GARs activity measured using a coupled enzyme assay with pyruvate kinase (PK) and lactate dehydrogenase (LDH). The continuous assay was recorded spectrophotometrically by measuring the consumption of NADH at 340 nm. The GARs reaction is highlighted with a *light blue roundrect*. The coupled reaction with PK and LDH is highlighted with a *light purple roundrect*. Purine biosynthesis enzymes are represented as *colored hexagons* as in Figure 1*A*. *B*, comparisons of the native bifunctional GARs/AIRs and single unit GARs Michaelis–Menten curves for ATP, glycine, and PRA, and enzyme kinetics parameters. Bifunctional GARs/AIRs curve and data points (mean with standard error) are shown in *pink* and the single unit GARs curve and data points are shown in *blue*. Specific activity, k_{cat}, K_m, and k_{cat}/K_m for the enzymes are recorded in the table.

15 μM for bifunctional GARs/AIRs, which was about two times lower than the value determined for the single unit GARs, which had a $K_{m\ app\_PRA}$ of 240 ± 15 μM. This reaction proceeded with increased specificity for the bifunctional GARs/AIRs (k_{cat}/K_{m_PRA}: (2.1 ± 0.2) × 10^5 M^{-1} s^{-1}), which was approximately three times higher than for single unit GARs (k_{cat}/K_{m_PRA}: (7.2 ± 0.6) × 10^4 M^{-1} s^{-1}).

In summary, the bifunctional GARs/AIRs specificity constants for ATP dephosphorylation and for the ligation of the glycyl group to PRA were considerably higher than for the single unit GARs, while the specificity constant for the phosphorylation of glycine was similar for the two proteins. These findings indicate that while the single unit GARs are sufficient to convert PRA to GAR, the dephosphorylation of ATP and ligation of the glycyl group to PRA are more efficient when the AIRs unit is attached.

Enzymatic parameters for GARs have been reported for the enzymes from three bacterial species, *A. aeolicus*, *E. coli*, and *Klebsiella pneumoniae*, as well as for two metazoan species, *Gallus gallus* and *H. sapiens* (Table 1). The *C. neoformans* bifunctional GARs/AIRs are most similar in overall specific activity (20.5 ± 0.27 U/mg) to the *E. coli* GARs for which a specific activity of 20.5 ± 1.5 U/mg has been reported. There is a key difference in enzyme specific activity between the fungal and metazoan enzymes; *C. neoformans* bifunctional GARs/AIRs have the highest reported specific activity (20.5 ± 0.27 U/mg) among the eukaryotic enzymes, 90 times greater than *H. sapiens* TrifGART (0.228 U/mg) and five times greater

Table 1
Comparison of kinetic parameters for GARs activity among enzymes from different species

Species	Enzyme form M.W.	Specific activity (U/mg)	k_{cat} (s^{-1})	K_m (ATP) (μM)	k_{cat}/K_m (ATP) (M^{-1} s^{-1})	K_m (Gly) (μM)	k_{cat}/K_m (Gly) (M^{-1} s^{-1})	K_m (PRA) (μM)	k_{cat}/K_m (PRA) (M^{-1} s^{-1})	Ref.
Cryptococcus neoformans	BiF GARs/AIRs 80 kDa	20.5 ± 0.27	27.3 ± 0.4	48 ± 3	(5.7 ± 0.4) × 10^5	496 ± 20	(5.5 ± 0.2) × 10^4	131 ± 15	(2.1 ± 0.2) × 10^5	This work
Homo sapiens	TriF GART 112 kDa	0.228	0.4	ND	ND	ND	ND	ND	ND	(54)
Gallus gallus	TriF GART 106 kDa	4.0	7.0	ND	ND	42 ± 5	1.7 × 10^5	41 ± 3	1.7 × 10^5	(55)
Klebsiella aerogenes	GARs 45 kDa	1.7	1.3	56	2 × 10^4	190	6 × 10^3	ND	ND	(56)
Escherichia coli	GARs 45 kDa	20.5 ± 1.5	15	170	9 × 10^4	270	5 × 10^4	70	2.1 × 10^5	(46)
Aquifex aeolicus	GARs 47.5 kDa	4.01	3.2	1000	3.2 × 10^3	590	5.4 × 10^3	ND	ND	(57)

Abbreviation: ND, no data provided.
Assay conditions were as follows: *C. neoformans* bifunctional GARs/AIRs and single unit GARs–100 mM Tris HCl, pH 8.0, 37 °C; *Homo sapiens* TrifGART (trifunctional GARs/AIRs/GART)–100 mM Tris HCl, pH 7.5, 37 °C; *G. gallus* TrifGART–10 mM Hepes, pH 7.5, 25 °C; *K. pneumoniae* GARs–85 mM Tris HCl, pH 8.0, 37 °C; *E. coli* GARs–100 mM Tris HCl, pH 8.0, 18 °C for Km and 37 °C for specific activity; *Aquifex aeolicus* GARs–50 mM Tris HCl, pH 7.9, 90 °C.
Reported values from publications are shown in dark gray. Values calculated from publication-reported enzyme functional parameters are shown in light gray.

than *G. gallus* TrifGART (4.0 U/mg). Related to this is the higher turnover number of the fungal enzyme compared with the metazoan enzymes; *C. neoformans* bifunctional GARs/AIRs turnover (27.3 ± 0.4 s^{-1}) is around 20 times greater than *H. sapiens* TrifGART (0.4 s^{-1}) and nearly four times greater than *G. gallus* TrifGART (7.0 s^{-1}). Interestingly, despite having a higher specific activity and faster turnover compared with the metazoan enzymes, a higher concentration of glycine and PRA are required to reach half maximal velocity for *C. neoformans* bifunctional GARs/AIRs compared with *G. gallus* TrifGART. The phosphorylation of glycine for *C. neoformans* bifunctional GARs/AIRs has a $K_{m\ app\_glycine}$ (496 ± 20 μM) that is around ten times higher than the reported $K_{m\ app\_glycine}$ (42 ± 5 μM) for *G. gallus* TrifGART. The ligation of the glycyl group to PRA for *C. neoformans* bifunctional GARs/AIRs has a $K_{m\ app\_PRA}$ (131 ± 15 μM) that is approximately three times higher than *G. gallus* TrifGART $K_{m\ app\_PRA}$ (41 ± 3 μM).

Overall, these comparisons indicate that there are functional differences between the fungal and metazoan enzymes with variations in the observed values of specific activity, k_{cat} and $K_{m\ app}$. Whether these functional differences may be exploited for antifungal development will depend on the identification of structural differences that can be exploited for the design of specific inhibitors.

Crystal structure of C. neoformans *GARs*

To compare the *C. neoformans* enzyme with the human ortholog, we aimed to determine the crystal structure of the *C. neoformans* bifunctional GARs/AIRs. As with human TrifGART, multiple attempts to crystallize the *C. neoformans* bifunctional GARs/AIRs as a single protein were unsuccessful (24). Therefore, the enzymatic units of GARs and AIRs were expressed and crystallized separately.

Purified recombinant *C. neoformans* GARs protein expressed in *E. coli* was successfully crystallized without ligands. The crystals diffracted to a resolution of 1.8 Å (Table S5). The crystal structure (PDB ID: 7LVO) contains one monomer consisting of 451 residues (excluding the 25 residue recombinant expression 6-His with a TEV protease cleavage site) per asymmetric unit, with four missing residues (position 196–199) in the model due to the absence of electron density, presumably due to flexibility. This enzyme belongs to the ATP grasp superfamily, a group of proteins that have a unique ATP-binding site known as the ATP grasp fold and that includes enzymes involved in cell metabolism, gluconeogenesis, fatty acid, and *de novo* purine biosynthesis (29). In this latter group, the ATP grasp fold has been identified in CAIR synthetase, as well as the formate-dependent forms of GAR transformylase and AICAR transformylase found exclusively in the Archaea and Bacteria (30–32).

Similar to GARs from other species, the *C. neoformans* structure has four domains: N (residues 34–160, five alpha-helices, four beta-strands); B (residues 161–237, three alpha-helices, three beta-strands); A (residues 238–381, six alpha-helices, five beta-strands); and C (residues 382–467, one alpha-helix, three beta-strands), which combine to form the binding sites for PRA, ATP, and glycine (Fig. 5*A*). A DALI (33) search of the Protein Data Bank (PDB) revealed that the *C. neoformans* GARs was most structurally similar to the human GARs, which is the only other available eukaryotic GARs structure (24). By superimposing the *C. neoformans* and human structure, there is a high level of overall conservation with a root mean square deviation (RMSD) of 1.25 Å. The binding sites of PRA, ATP, and glycine for the *C. neoformans* and human structure are similar and key residues for binding are well conserved.

Based on the conservation of key binding residues of the *H. sapiens* and *C. neoformans* structures, the key binding residues for the *C. neoformans* enzyme can be predicted based on the structural superimposition. The PRA-binding site in the *C. neoformans* enzyme includes Arg48 and Glu49 in the N domain, Asp338 in the A domain, and Arg427 in the C domain (24). The Mg^{2+}/ATP-binding site includes Lys262

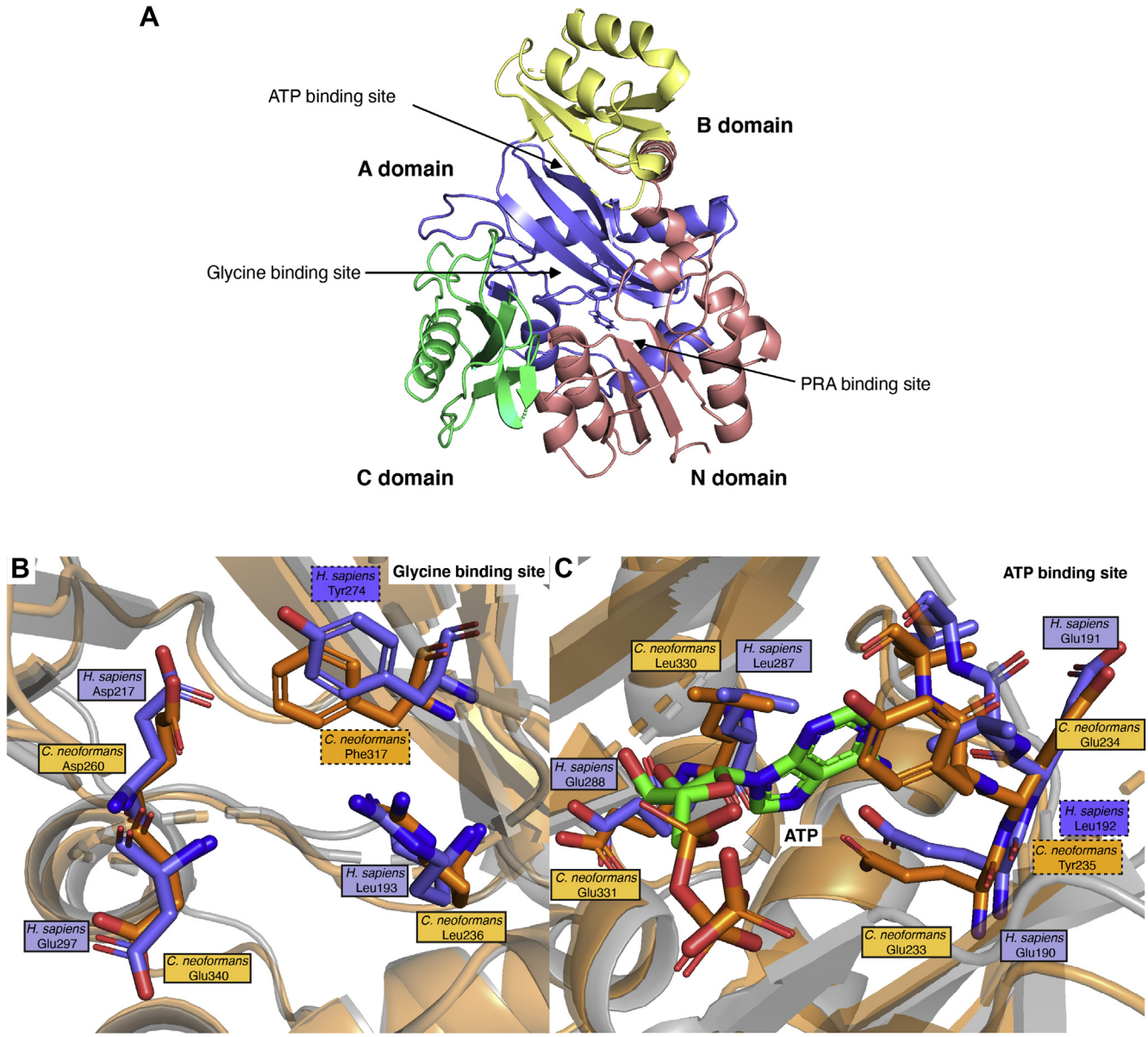

Figure 5. Crystal structure of *Cryptococcus neoformans* GARs. *A*, Four domains of *C. neoformans* GARs. The N domain is shown in *pink*, *A* in purple, *B* in *yellow*, and *C* in *green*. *B* and *C*, comparison of the glycine and ATP-binding sites from *C. neoformans* and *H. sapiens* GARs. The *C. neoformans* GARs model is shown in *orange*, the *H. sapiens* GARs model (PDB ID: 2QK4) is shown in *purple*. The side chains of the residues that make up the binding site are shown as a stick representation. The amino acid differences identified in these binding sites are highlighted in *boxes* with *dotted lines*. The green ATP molecule is from the *H. sapiens* GARs structure.

(B domain). The glycine-binding site includes Asp260 (B domain), Arg335 (A domain), Asp338 (A domain), and Glu340 (A domain). These residues are all 100% conserved in the human ortholog.

Despite the high level of conservation of key binding residues with the human enzyme, analysis of the binding sites of GARs identified two amino acid differences, one in the glycine-binding site and the other in the ATP-binding site, at the position where the adenine ring would fit (Fig. 5, *B* and *C*). The first amino acid difference was identified at the glycine-binding site, where Phe317 of *C. neoformans* GARs corresponds to Tyr274 in human GARs. This residue interacts with the ammonium group of glycine (Fig. 5*B*). The side chains of both amino acids have a similar orientation, indicating that the position of the amino acid could be crucial for glycine attachment. Phenylalanine and tyrosine both contain an aromatic ring, the only difference being the presence of the hydroxyl group in tyrosine, causing it to be more polar. The difference in polarity might be used to influence specific inhibitor design to the *C. neoformans* enzyme. The two other major fungal pathogens, *Candida albicans* and *Aspergillus fumigatus*, also have the same corresponding phenylalanine residue (Fig. S2), thus exploiting this feature for antifungal drug design might enable broad spectrum efficacy.

The second amino acid difference corresponds to Tyr235 at the ATP-binding site of *C. neoformans* GARs, where the corresponding residue is Leu192 in human GARs (Fig. 5*C*). Although the side chains of Tyr235 and Leu192 are oriented in

a similar direction, their side chains have different properties. Tyrosine has an aromatic amphipathic side chain, while leucine has an aliphatic nonpolar side group. The tyrosine also extends into the adenine-binding pocket by approximately 5 Å more than leucine; a specifically designed inhibitor could utilize the differences in the properties of the side chain, as well as the size of the binding pocket, to favor the *C. neoformans* binding site over the *H. sapiens* enzyme binding site. This amino acid is not conserved across the three major fungal pathogens; *A. fumigatus* has the same tyrosine, while *C. albicans* has a phenylalanine (Fig. S2). However, tyrosine and phenylalanine are much more similar than a leucine, thus designing an inhibitor to fit this binding pocket for fungal pathogens might still be possible.

Crystal structure of C. neoformans *AIRs*

The purified recombinant *C. neoformans* AIRs expressed in *E. coli* was successfully crystallized without ligands. The crystals diffracted to a resolution of 2.2 Å and the crystal structure (PDB ID: 7LVP) contained one monomer per asymmetric unit (Table S6). Excluding the His-tag (25 residues), each monomer consists of 307 residues, forming 11 alpha-helices and 9 beta-strands (Fig. 6). Residues 91–98 and residues 122–137 were not modeled (Fig. S3) as there was no electron density observed for these regions; they are presumably disordered. Based on mass photometry data, this protein exists as a dimer, consistent with structures of AIRs in other species (23–25). The pair of monomers forming the dimer in the crystals is related by a crystallographic twofold axis.

Structural analysis of the *C. neoformans* AIRs indicated that it belongs to the PurM superfamily, which includes AIRs from other species as well as the ATPase domain of FGAM synthetase. The dimer has one binding site for ATP and one for the substrate FGAM, each of which lies in the homodimer interface of the four beta-strands from monomer A and four beta-strands of monomer B. Based on the superimposition of ligand-bound *T. thermophilus* AIRs and *C. neoformans* AIRs, and the mechanism proposed previously for the *T. thermophilus* enzyme, the key binding residues for ATP and FGAM are fully conserved. In the *C. neoformans* AIRs structure, ATP would be predicted to bind to conserved residues Asp77 (monomer A), Asp48 (monomer B), Glu124 (B), Gly123 (B), Asp90 (B), and a Mg^{2+} ion would be bound by Asp77 (A) and His231 (A) at the dimer interface of the *C. neoformans* AIRs. FGAM is predicted to be bound by the conserved residues Gly49 (both monomers A and B), Val50 (B), Tyr91 (B), Ser174 (A and B), and Asn175 (B), causing a conformational change in the N-terminal region of the enzyme. Based on previous mechanism proposed for *T. thermophilus* AIRs, the correct positioning of the substrates in the *C. neoformans* AIRs enables the hydrolysis of ATP to activate the FGAM formyl oxygen, which is coordinated by the conserved Gly46 (A) and Glu124 (B); the nitrogen then triggers a nucleophilic substitution on the activated formyl oxygen and transfers the oxygen to the phosphate formed during ATP hydrolysis. This reaction closes the five-membered imidazole ring of the purine base and forms AIR (20).

Based on a DALI search of the PDB, the top hit is human AIRs as expected as this is the only other eukaryotic structure available for this enzyme. A structural alignment of the monomeric units of *C. neoformans* and human AIRs shows high conservation, with an RMSD of 0.99 Å. However, when the dimeric unit of the *C. neoformans* AIRs is structurally

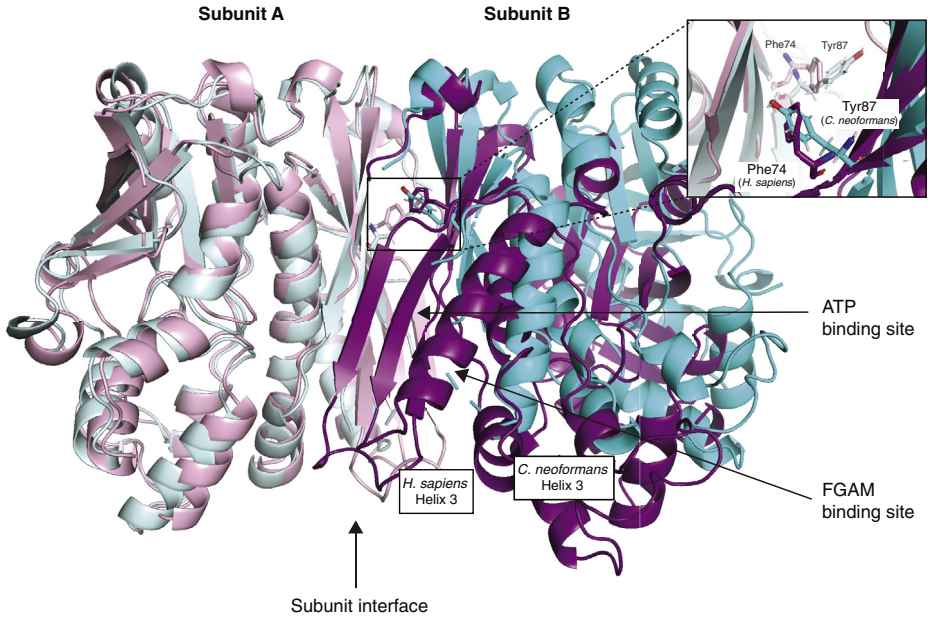

Figure 6. Comparison of the dimeric structures of *C. neoformans* and *H. sapiens* AIRs. The *C. neoformans* AIRs model is shown in *pale cyan* (subunit A) and cyan (subunit B). The *H. sapiens* AIRs model (PDB ID: 2QK4) is shown in *light pink* (subunit A) and *deep purple* (subunit B). Binding sites of human AIRs are indicated in the model. Residue modification from Tyr87 to Phe74 is highlighted in the model with a *black box* and is in stick representation. The superposition of the dimers yields an RMSD value of 2.55 Å.

superimposed with the human AIRs dimer, the RMSD is increased to 2.55 Å, suggesting a different orientation of the monomers in each dimeric unit (Fig. 6). By aligning one monomer of the dimer unit from *C. neoformans* and human AIRs, and using the third alpha helix as an anchor, the orientation of second monomers differs by an angle of 22.2° (Fig. 6). Additional investigation of the dimer interface (using PISA (34)) reveals that there are more residues that form hydrogen bonds in the dimer interface for the *H. sapiens* AIRs compared with the *C. neoformans* AIRs, which could explain the differences in dimer arrangement. Furthermore, there is a residue modification in the dimer-interacting beta-strands of the *C. neoformans* AIRs from a Tyr87 to a Phe74 in *H. sapiens* AIRs that might have caused the change in dimer conformation (Fig. 6). There could be potential for drugs to target the differences in the interface, disrupting dimer formation and by extension creation of the active site.

Discussion

Unlike a number of *de novo* purine biosynthesis enzymes that have alternative enzymes that can perform equivalent biochemical roles, there are no alternative enzymes that perform the role of GARs or AIRs (21). In the Archaea and the Bacteria, these conserved GARs or AIRs proteins are almost exclusively encoded by individual genes. Rare exceptions do exist, such as the intracellular pathogens of the *Francisella* genus in the Bacteria where GARs and a different enzyme in the pathway, SAICAR synthetase, are fused together. In fungi, the genes encoding GARs and AIRs are fused, and this fusion is later expanded with the addition of GAR_T in the Metazoa and some protists. This addition of GAR_T, an entire enzymatic unit almost 30 kDa in size, is a major structural difference that may potentially be exploited alongside smaller key amino acid changes in the development of new, fungal-specific purine biosynthesis inhibitors, to treat disseminated life-threatening mycoses without interfering with the host purine metabolism.

Deletion analyses of the *ADE5,7* gene encoding *C. neoformans* GARs/AIRs revealed several growth phenotypes. Adenine supplementation was required for growth of the *ade5,7Δ* mutant but guanine supplementation alone was unable to restore growth. Adenine/adenosine deaminase in *C. neoformans* enables the conversion of adenine/adenosine into hypoxanthine/inosine, which in turn can be converted into guanine. In contrast, there are no enzymes that can convert guanine into hypoxanthine, thus the inability of guanine to restore growth to the mutant. Unlike the *imd1Δ*, *gua1Δ*, *ade12Δ*, and *ade13Δ* purine biosynthesis mutants previously studied in *C. neoformans* that could not grow on unsupplemented YPD, the *ade5,7Δ* mutant was able to grow under this condition, demonstrating its ability to utilize purines in the YPD media (13–15). However, mechanisms influencing utilization of purines in YPD are still unknown.

Major virulence trait production of the *ade5,7Δ* mutant was similar to the wild-type strain, unlike the *imd1Δ*, *gua1Δ*, *ade12Δ*, and *ade13Δ* purine biosynthesis mutants, which were impaired in melanin, capsule, and protease production (13–15). However, consistent with the other purine enzyme deletion mutants, mice infected with the *ade5,7Δ* strain remained healthy at the end of the experiment and the infection was cleared from all major organs. This result supports the model that the reduced virulence of purine biosynthetic mutants is primarily due to the inability to synthesize purines *de novo* during infection of the purine-poor central nervous system and not due to diminished virulence trait production (11).

A comparative analysis of *C. neoformans* bifunctional GARs/AIRs and its GARs unit alone revealed differences in enzyme kinetic parameters. The single unit GARs have a 3-fold lower preference for PRA compared with the bifunctional enzyme. This decreased preference for PRA in the absence of the AIRs unit suggests that sections of the protein that promote PRA binding may have been removed. The only other eukaryote in which the $K_{m\ app\_PRA}$ has been determined, *G. gallus* TrifGART, has similar specificity for PRA compared with the *C. neoformans* bifunctional GARs/AIRs, supporting the model that the inclusion of the second enzymatic unit may have an effect on PRA binding. Comparison between the *C. neoformans*, *G. gallus*, and *H. sapiens* enzymes revealed differences in substrate specificities, which could suggest that the substrates might interact differently with the binding sites. The lower affinity for substrate binding observed for the *C. neoformans* enzyme suggests that inhibitors that are substrate analogs may be less suitable, as there is a higher likelihood for the *H. sapiens* enzyme to bind these substrate analogs more strongly due to its higher affinity. Instead, specifically designed inhibitors could target the unique binding properties of the *C. neoformans* enzyme, which were revealed through structure determination of the *C. neoformans* GARs unit. In consideration of differing assay conditions in various organisms, direct comparison of these kinetic parameters may be limited and studies to investigate each specific condition could be instigated.

Although the biochemical characterization of AIRs, the second enzyme unit of bifunctional GARs/AIRs, has the potential to reveal functional differences as well, the unavailability of the substrate FGAM from commercial sources and the complexity of FGAM chemical synthesis required to make it ourselves precluded these functional assays for AIRs being performed. However, in the future, there may be opportunities to investigate this activity. Despite this lack of AIRs enzyme kinetic data, we are still well informed about the key differences in the protein through the determination of the crystal structure. While recombinant GARs/AIRs did not crystallize likely due to the presence of a flexible linker between the two enzymatic units, expression of the two enzymatic units as separate constructs enabled successful crystallization. The same strategy had also been employed in the determination of these structures from the *H. sapiens* enzyme (24). In addition, crystallization of these proteins with ligands was attempted; however, diffracted crystals did not contain the ligands of interest.

The GARs unit crystals diffracted to a resolution of 1.8 Å and the structure was refined to R_{free} of 0.28. After data quality

analysis, it seems that the higher R_{free} and R_{work} values for this model are likely due to a large disordered region between residues 194 and 230 in the B-domain, which is known to be flexible based on previous structures. As the core of the protein could be modeled reliably, accurate comparisons of the *C. neoformans* GARs model can still be made with the *H. sapiens* GARs crystal structure. Despite the overall *C. neoformans* structure being highly similar to *H. sapiens*, a closer analysis of the binding sites for glycine and ATP identified two important amino acid residue differences: *H. sapiens* Tyr274 corresponds to *C. neoformans* Phe317 and *H. sapiens* Leu192 corresponds to *C. neoformans* Tyr235. The Leu192 to Tyr235 residue mutation results in a change in the size of the binding pocket and has differing side chain properties that have more potential to be exploited in drug design, by creating an inhibitor that can bind specifically to the fungal-binding site. Functional catalytic data could not be directly correlated with structural information as there is limited kinetic data available for the human ortholog that only reported specific activity for GARs.

The *C. neoformans* AIRs unit crystals diffracted to a resolution of 2.2 Å and the structure was refined to an R_{free} of 0.26. The monomer of the *C. neoformans* enzyme is very similar to its ortholog from *H. sapiens*, with the ATP and FGAM-binding sites highly conserved; however, there is a distinct difference in the dimeric arrangement. The variation in the dimer arrangement of the *C. neoformans* AIRs is likely due to part of the interface observed in the human enzyme being disordered (residues 91–98 and residues 122–137 based on truncated AIRS domain construct) (Fig. S3). As a consequence, the monomers are held closer together in the human AIRs (Fig. 6). Another reason for this difference could be due to the amino acid residue modification from a Tyr87 to a Phe74 in the human enzyme, which could push monomers within the dimer further apart in the fungal enzyme (Fig. 6). As the dimer interface is crucial for the enzymatic function, a molecule could potentially be designed to specifically target the *C. neoformans* AIRs dimer interface.

In short, this study reports a multifaceted characterization of *C. neoformans* bifunctional GARs/AIRs through gene deletion studies of *ADE5,7*, the first enzyme kinetic analysis of eukaryotic GARs outside the Metazoa and the first structure determination of both GARs and AIRs from a nonhuman eukaryote. Not only could we utilize the subtle differences identified through functional and structural comparison for future drug design, we could also use the similarities as a tool to possibly gain better insights of the eukaryotic GARs and AIRs biochemical and structural mechanisms, which could be relevant even for noneukaryotic organisms as these enzymes are present across all domains of life.

Experimental procedures

Bioinformatic analysis

The *ADE5,7* gene and protein sequences were obtained from the *C. neoformans* H99O-type strain genome published by Janbon *et al.* (35). The gene encoding GARs and AIRs was identified in the *C. neoformans* genome *via* tBLASTn search using the *S. cerevisiae* homolog. Reciprocal analysis *via* BLASTp was performed using the translated product of *CNAG_06314* to query the *S. cerevisiae* genome. Sequence alignments of GARs and AIRs from *C. neoformans*, *S. cerevisiae*, and *H. sapiens* were performed using ClustalW v1.4 (MacVector Inc).

Media and strains

All strains are listed in Table S1. Wild-type (*C. neoformans* H99O) and *ade5,7Δ+ADE5,7* complemented strains were grown in yeast peptone dextrose (YPD) media (2% bactopeptone, 1% yeast extract, 2% glucose, 2% agar) at 30 °C, unless otherwise stated. The *ade5,7Δ* mutant was grown in yeast nitrogen base (YNB) media (0.45% yeast nitrogen base without amino acids and ammonium sulfate, 10 mM $(NH_4)_2SO_4$, 2% glucose, 2% agar) supplemented with 1 mM adenine at 30 °C, unless otherwise stated. Mach1 *E. coli* (Thermo Fisher Scientific) strains were used for cloning the expression vectors and BL21 *E. coli* (Agilent Technologies) strains were used for protein expression. Mach1 *E. coli* was grown on lysogeny broth (LB) agar (1% tryptone, 0.5% yeast extract, 1% sodium chloride, 2% agar) supplemented with 100 μg/ml ampicillin at 37 °C. BL21 *E. coli* was grown in autoinduction growth media (0.5% yeast extract, 1% tryptone, 2%, 0.5% glycerol, 0.05% glucose, 0.2% lactose, 0.5 M $(NH_4)_2SO_4$, 0.5 M KH_2PO_4, 1 M Na_2HPO_4, 1 mM $MgSO_4$) for protein expression.

Creating ADE5,7 *gene deletion and complementation strains*

All primers (IDT) used in this study are listed in Table S2 and plasmids in Table S3. Phusion High Fidelity polymerase (New England Biolabs) was used for generation of all PCR amplicons. Genomic DNA extracted from *C. neoformans* wild-type was used as a template to amplify 5′ upstream and 3′ downstream regions of *ADE5,7* and pJAF1 was used to amplify *NEO* (36). 1 kb upstream of *ADE5,7* (UQ4315, UQ3880), the *NEO* marker (UQ3881, UQ3882), and 1 kb downstream of *ADE5,7* (UQ3883, UQ4316) were combined using NEBuilder HiFi DNA Assembly (New England Biolabs) to create a deletion construct that was cloned into pBlueScriptII SK(-) to create pSMHC8. CLC Genomics Workbench 7.5 (CLC bio) was used to analyze sequencing data generated from the Australian Genome Research Facility (AGRF).

Biolistic transformation of the deletion construct was performed using a BioRad He-1000 Biolistic Device (37) into *C. neoformans* H99O strain on YNB media supplemented with 10 mM adenine, 1 M sorbitol, and 5 μg/ml W7 hydrochloride (38). Transformants were subsequently selected on YNB media supplemented with 10 mM adenine and 100 μg/ml G418. G418-resistant colonies were characterized *via* diagnostic PCR (UQ3132 and UQ1036) and tested for adenine auxotrophy on YNB media. To verify that *ADE5,7* was successfully deleted from *C. neoformans*, CTAB extracted DNA from the *ade5,7Δ* mutants (39) was digested with EcoRV and NcoI (New England Biolabs), then run on an agarose gel at 20 V overnight. DNA from the agarose gel was Southern blotted to a Hybond-

XL membrane (GE Healthcare) (40). The *ADE5,7* probe (UQ3884 and UQ3885) was radioactively labeled using DECAprime II kit (Thermo Fisher Scientific) and dCTP [α-^{32}P] (PerkinElmer). The blots were hybridized with the radioactively labeled probe overnight at 65 °C, then washed with 0.1% SDS, 2× SSC buffer, exposed on Fuji Super RX medical X-ray film (Fujifilm), and was visualized after development.

Complementation of the *ade5,7*Δ mutant was performed through reintroduction of *ADE5,7* at the Safe Haven locus in chromosome 1 (26). The region consisting of 5′ region of *ADE5,7,* the *ADE5,7* CDS, *and 3′* region of *ADE5,7* (UQ4315, UQ4316) was cloned into Safe Haven, targeting pSDMA25, to create pSMHC1. pSMHC1 was linearized with PacI and transformed into the Safe Haven location of *ade5,7*Δ mutant. Transformants were selected on YPD media supplemented with 100 μg/ml nourseothricin (*NAT*). Transformant colonies were screened by diagnostic PCR (UQ1768, UQ2962, UQ2963, and UQ3348) and for adenine prototrophy (26). Precise integration of *ADE5,7* at the Safe Haven location was verified by Southern blot with the same probe used for verifying the *ade5,7*Δ mutant.

Phenotype and virulence assays

C. neoformans strains were suspended in 1 ml of dH_2O and diluted to OD_{600} = 1.0. For observation of adenine auxotrophy, the cell suspension was diluted by 10-fold serially to 10^{-4} and spotted on YPD, YNB, and YNB supplemented with 1 mM adenine. Plates were incubated at 30 °C and 37 °C. Images were taken 48 h postincubation. All growth spotting assays were done in triplicate.

For observation of virulence trait production, 3 μl of 10^{-1} dilution suspension was spotted on media as follows: L-DOPA agar supplemented with 10 mM asparagine for melanin production (41); Christensen's urea agar for urease production (42); Sabouraud's dextrose agar supplemented with 8% egg yolk for phospholipase B production (43); and YNB complete agar supplemented with 1% BSA (BSA, Sigma-Aldrich) for protease production. All media used for virulence assays were supplemented with 1 mM adenine to compensate for the adenine auxotrophy of the *ade5,7Δ* mutant. Plates were incubated at 30 °C and 37 °C. Images were taken 48 h postincubation for L-DOPA agar, Christensen's urea agar, and BSA agar while images were taken 72 h postincubation for egg yolk agar. All virulence trait production spotting assays were done in triplicate.

For capsule assays, strains were grown in RPMI 1640 (Life Technologies) supplemented with 2% glucose, 10% foetal bovine serum (Life Technologies), and 1 mM adenine in a shaking incubator at 30 °C or 37 °C. After 24 h growth, cells were stained with India ink (BD Diagnostics), viewed, and imaged using a Leica DM2500 microscope and DFC425C camera (Leica). Five images were photographed for each strain. The whole cell and cell body diameter of 5 cells from each image were measured using the ruler tool in Adobe Photoshop CC (Adobe Systems), and capsule measurement was presented as a relative percentage of cell size. The capsule assays were performed in triplicate. A one-way ANOVA test with Sidak's posttest was used to determine significance of differences in capsule sizes between strains.

Mouse virulence experiments

Ten 6-week-old mice were intranasally infected with 5×10^5 cells of *C. neoformans* H99O wild-type strain, the *ade5,7*Δ mutant, and *ade5,7Δ+ADE5,7* complemented strain. Five mice were housed in an IVC cage, which was lined with Bed-o'Cobs 1/8" bedding (The Andersons), Crink-L'Nest nesting material (The Andersons), and cardboard. Mice were provided with constant supply of Rat and Mouse Cubes (Specialty Feeds) and drinking water. After infection, the mice were monitored for signs of *C. neoformans* infection, scored, and weighed daily. When the mice lost 20% of their starting body weight or showed severe symptoms, they were euthanized by carbon dioxide inhalation. The spleen, liver, kidney, lungs, and brains were collected and homogenized using TissueLyser II (QIAGEN). The organ suspensions were serially diluted and spotted on YPD agar supplemented with 100 μg/ml ampicillin, 50 μg/ml kanamycin, and 25 μg/ml chloramphenicol, to prevent bacterial contamination. After 48 h, the colonies were counted to calculate the organ burden. The survival curves and organ burden plots were plotted using Graphpad Prism 7.0 (GraphPad Software Inc). The log rank test and a one-way ANOVA with Tukey's multiple comparisons test were used to determine the significance of survival and the organ burden, respectively.

Ethics statement

This study was carried out in strict accordance with the recommendations in the Australian Code of Practice for the Care and Use of Animals for Scientific Purposes by the National Health and Medical Research Council. The protocol was approved by the Molecular Biosciences Animal Ethics Committee of The University of Queensland (AEC approval number: SCMB/010/17). Infection was performed under methoxyflurane anesthesia, and all efforts were made to minimize suffering through adherence to the Guidelines to Promote the Wellbeing of Animals Used for Scientific Purposes as put forward by the National Health and Medical Research Council.

Protein expression and purification

The *ADE5,7* ORF was amplified from three custom gBlock gene fragments (uqg19, uqg20, uqg21; Table S4) (IDT), using Phusion High Fidelity polymerase in a two-step amplification. The ORF was amplified in two fragments (UQ3890 and UQ3869, UQ3868 and UQ3891) and then a second round of overlap PCR (UQ3890 and UQ3891) to form the entire *ADE5,7* ORF. The amplified *ADE5,7* ORF was digested with BamHI (New England Biolabs) then cloned into BamHI/SspI-cut pMCSG7 to introduce the His-tag into the ORF and create the protein expression plasmid pSMHC2, which was verified by Sanger sequencing. The ORF for the GARs region of *ADE5,7* was amplified from

pSMHC2 using primers UQ4282 and UQ4283, then cloned into the SspI/BamHI cut pMCSG7 using NEBuilder HiFi DNA Assembly, to create the plasmid pSMHC10, which was verified by sequencing. The ORF for the AIRs region of *ADE5,7* was amplified from pSMHC2 using primers UQ4284 and UQ4285, then cloned into the SspI/BamHI cut pMCSG7 using NEBuilder HiFi DNA Assembly to create the plasmid pSMHC11, which was verified by Sanger sequencing.

Expression constructs were transformed into BL21(DE3) *E. coli* and grown in a shaking incubator at 37 °C for 3 h in autoinduction growth media (44) supplemented with 100 μg/ml ampicillin until OD_{600} reached a value of 1.0. A 4 L culture was then grown in an incubator shaking at 220 rpm at 18 °C overnight. The cells pelleted from the culture was resuspended in lysis buffer (50 mM HEPES, 300 mM NaCl, 1 mM DTT, 100 mM phenylmethylsulfonyl fluoride). The cells were lysed by sonication and the lysate was collected by centrifugation at 16,000 rpm. A HisTrap Fast Flow column (GE Healthcare) was used for purification and the protein was eluted using an elution buffer containing 150 mM imidazole (50 mM HEPES, 300 mM NaCl, 150 mM imidazole). The eluted protein was then concentrated using an Amicon Ultra 15 ml centrifugal filter device (Merck Millipore). The protein was further purified using a Superdex 200 Increase column at a rate of 2.5 ml/min (GE Healthcare) that was equilibrated with gel filtration buffer (10 mM HEPES pH 7.5, 150 mM NaCl, 1 mM DTT) using an ÄKTA pure FPLC system (GE Healthcare) to separate the protein by size. The fractions of the eluted protein corresponding to a single peak were pooled and concentrated to 10 mg/ml. The purified protein was stored at −80 °C for future use.

Mass photometry

A Refeyn OneMP instrument (Refeyn Ltd) was used to measure the oligomeric states of the proteins in solution (45). Ten microliter of gel filtration buffer followed by 1 μl of the protein solution was applied to the drop to a final concentration of 100 nM and 6000 frames were recorded. The calibration curve was obtained by using three protein standards (66, 146, and 480 kDa) (Thermo Fisher Scientific).

GARs enzyme kinetic assays

For the synthesis of PRA, 5 mg of ribose-5-phosphate, 250 μl of NH_4Cl, and 50 μl 5 M KOH were incubated at 37 °C for 30 min and the product was quantified according to Schendel and others (28). The GARs activity was monitored spectrophotometrically using a Cary60 UV-Vis spectrophotometer (Agilent). All enzyme activity assays were performed in biological triplicates. The standard assay was performed based on the approach used previously for the *E. coli* GARs, with the modification running the assay at 37 °C using 0.0175 mg GARs and 2 mM PRA (46). As it is unstable at higher temperatures, the reaction was initiated with the addition of PRA rather than the addition of the enzyme. GARs activity was determined by following the oxidation of NADH at 340 nm (ε340 = 6220 M^{-1} cm^{-1}). The concentration ranges for measuring the K_m of substrates ATP, PRA, and glycine ranged from 4 μM to 2000 μM, 16 μM to 2000 μM, and 8 μM to 4000 μM. Enzyme kinetic data were processed and fit to the Michaelis–Menten equation using Graphpad Prism 7.0 (GraphPad Software Inc).

Crystallization and structure determination of C. neoformans *GARs and AIRs*

All crystallization attempts were performed *via* hanging drop vapor diffusion method. Eight commercial screening plates, Grid Screen Sodium Malonate, Grid Screen Ammonium Sulfate, Grid Screen Sodium chloride, Grid Screen PEG/LiCl, PEGION, and PEGRX (Hampton Research), JSCG, Morpheus, PACT, PROPLEX, and ShotGun (Molecular Dimensions) were used to screen crystallization conditions with protein concentrations of 10 mg/ml. A Mosquito crystallization robot (TTP Labtech) was used to set up screening plates. Each drop contained 100 nl protein solution and 100 nl reservoir solution inverted over 100 μl reservoir solution. The crystallization screens were incubated at 20 °C and monitored by the Rock Imager system (Formulatrix). The GARs protein crystallized in 0.1 M sodium citrate, pH 5.0, 30% v/v MPEG550, and the AIRs protein crystallized in 0.1 M SPG (succinic acid, sodium dihydrogen phosphate, and glycine in ratio of 2:7:7), 25% w/v PEG1500.

Diffraction data were collected on the MX2 beamline of the Australian Synchrotron. Data were collected using Blu-Ice (47), and processed and scaled using XDS (48) and Aimless (49). The *C. neoformans* GARs structure was solved by molecular replacement using Phaser (50) in the PHENIX suite version 1.14 (51), with *H. sapiens* GARs (PDB ID: 2QK4) as the template model. The *C. neoformans* GARs model was refined using data between 38 Å and 2 Å resolution, and in-between rounds of refinement model building were conducted with Coot version 0.8.9.2 (52). The data collected were analyzed using Phenix xtriage, verifying the absence of twinning symmetry, outliers, and abnormalities. The *C. neoformans* AIRs were solved by molecular replacement using Phaser (50) in the PHENIX suite version 1.14 (51) with the *Neisseria gonorrhoeae* AIRs (PDB ID: 5VK4) as the template model. The AIRs model was refined using data between 42 Å and 2.23 Å resolution, and in-between rounds of refinement model building were conducted with Coot version 0.8.9.2 (52). Structures in the PDB similar to *C. neoformans* GARs and AIRs were identified using DALI (33). *C. neoformans* and *H. sapiens* enzyme structures were superimposed using the Pymol align command. Interacting residues were analyzed using PISA (53).

Data availability

The atomic coordinates and structure factors (PDB ID: 7LVO, 7LVP) have been deposited in the Protein Data Bank (https://www.rcsb.org/).

Supporting information—This article contains supporting information (26, 58).

Acknowledgments—Crystallization was conducted at the University of Queensland Remote Operation Crystallization and X-ray

Diffraction Facility (UQ ROCX). X-ray diffraction data was collected on the MX2 beamline at the Australian Synchrotron, Victoria, Australia. The authors acknowledge the facilities, and the scientific and technical assistance, of the Australian Microscopy & Microanalysis Research Facility at the Centre for Microscopy and Microanalysis, The University of Queensland.

Author contributions—S. M. H. C., U. K., B. K., and J. A. F. conceptualization; S. M. H. C. and Z. L. data curation; S. M. H. C., M. S. I. W., B. Y. J. L., U. K., B. K., and J. A. F. formal analysis; J. A. F. funding acquisition; S. M. H. C., M. S. I. W., Z. L., and B. Y. J. L. investigation; S. M. H. C. and Z. L. methodology; S. M. H. C. project administration; J. A. F. resources; Z. L., U. K., B. K., and J. A. F. supervision; Z. L., U. K., B. K., and J. A. F. validation; S. M. H. C. and M. S. I. W. visualization; S. M. H. C. writing–original draft; S. M. H. C., M. S. I. W., U. K., B. K., and J. A. F. writing–review and editing.

Funding and additional information—This research was supported by the National Health and Medical Research Council, http://www.nhmrc.gov.au/, APP1130192 to J. A. F.

Conflict of interest—The authors declare that they have no conflicts of interest with the contents of this article.

Abbreviations—The abbreviations used are: AIR, phosphoribosyl-aminoimidazole; AIRs, AIR synthetase; FGAM, formylglycinamidine; FGAMs, FGAM synthetase; FGAR, phosphoribosyl-formylglycinamide; GAR, phosphoribosyl-glycinamide; GARs, GAR synthetase; IMAC, immobilized metal affinity chromatography; k_{cat}, turnover number; LDH, lactate dehydrogenase; L-DOPA, l-3,4-dihydroxyphenylalanine; *NAT*, nourseothricin; N^{10}-fTHF, 10-formyltetrahydrofolate; N^{10}-fTHF-GAR$_T$, GAR transformylase; PDB, Protein Data Bank; PK, pyruvate kinase; PRA, phosphoribosyl-amine; PRPP, phosphoribosyl-pyrophosphate; PRPP$_A$, PRPP amidotransferase; TrifGART, trifunctional GART; RMSD, root mean square deviation; SAXS, small-angle X-ray scattering; SEC, size-exclusion chromatography; SPG, succinic acid, sodium dihydrogen phosphate, and glycine; YNB, yeast nitrogen base; YPD, yeast peptone dextrose.

References

1. Elion, G. B., Furman, P. A., Fyfe, J. A., de Miranda, P., Beauchamp, L., and Schaeffer, H. J. (1977) Selectivity of action of an antiherpetic agent, 9-(2-hydroxyethoxymethyl) guanine. *Proc. Natl. Acad. Sci. U. S. A.* **74**, 5716–5720
2. Elion, G. B., Kovensky, A., and Hitchings, G. H. (1966) Metabolic studies of allopurinol, an inhibitor of xanthine oxidase. *Biochem. Pharmacol.* **15**, 863–880
3. Hamilton, L., and Elion, G. B. (1954) The fate of 6-mercaptopurine in man. *Ann. N. Y. Acad. Sci.* **60**, 304–314
4. Roemer, T., and Krysan, D. J. (2014) Antifungal drug development: Challenges, unmet clinical needs, and new approaches. *Cold Spring Harb. Perspect. Med.* **4**, a019703
5. Rajasingham, R., Smith, R. M., Park, B. J., Jarvis, J. N., Govender, N. P., Chiller, T. M., Denning, D. W., Loyse, A., and Boulware, D. R. (2017) Global burden of disease of HIV-associated cryptococcal meningitis: An updated analysis. *Lancet Infect. Dis.* **17**, 873–881
6. Fanos, V., and Cataldi, L. (2000) Amphotericin B-induced nephrotoxicity: A review. *J. Chemother.* **12**, 463–470
7. Loyse, A., Thangaraj, H., Easterbrook, P., Ford, N., Roy, M., Chiller, T., Govender, N., Harrison, T. S., and Bicanic, T. (2013) Cryptococcal meningitis: Improving access to essential antifungal medicines in resource-poor countries. *Lancet Infect. Dis.* **13**, 629–637
8. Friese, G., Discher, T., Füssle, R., Schmalreck, A., and Lohmeyer, J. (2001) Development of azole resistance during fluconazole maintenance therapy for AIDS-associated cryptococcal disease. *AIDS* **15**, 2344–2345
9. Brüggemann, R. J., Alffenaar, J. W., Blijlevens, N. M., Billaud, E. M., Kosterink, J. G., Verweij, P. E., and Burger, D. M. (2009) Clinical relevance of the pharmacokinetic interactions of azole antifungal drugs with other coadministered agents. *Clin. Infect. Dis.* **48**, 1441–1458
10. Perfect, J. R., Dismukes, W. E., Dromer, F., Goldman, D. L., Graybill, J. R., Hamill, R. J., Harrison, T. S., Larsen, R. A., Lortholary, O., Nguyen, M.-H., Pappas, P. G., Powderly, W. G., Singh, N., Sobel, J. D., and Sorrell, T. C. (2010) Clinical Practice Guidelines for the management of cryptococcal disease: 2010 update by the Infectious Diseases Society of America. *Clin. Infect. Dis.* **50**, 291–322
11. Thane Eells, J., and Spector, R. (1983) Purine and pyrimidine base and nucleoside concentrations in human cerebrospinal fluid and plasma. *Neurochem. Res.* **8**, 1451–1457
12. Chitty, J. L., Edwards, D. J., Robertson, A. A. B., Butler, M. S., Duley, J. A., Cooper, M. A., and Fraser, J. A. (2019) Quantitation of purines from pigeon guano and implications for *Cryptococcus neoformans* survival during infection. *Mycopathologia* **184**, 273–281
13. Morrow, C. A., Valkov, E., Stamp, A., Chow, E. W., Lee, I. R., Wronski, A., Williams, S. J., Hill, J. M., Djordjevic, J. T., Kappler, U., Kobe, B., and Fraser, J. A. (2012) *De novo* GTP biosynthesis is critical for virulence of the fungal pathogen *Cryptococcus neoformans*. *PLoS Pathog.* **8**, e1002957
14. Blundell, R. D., Williams, S. J., Arras, S. D., Chitty, J. L., Blake, K. L., Ericsson, D. J., Tibrewal, N., Rohr, J., Koh, Y. Q., Kappler, U., Robertson, A. A., Butler, M. S., Cooper, M. A., Kobe, B., and Fraser, J. A. (2016) Disruption of de Novo adenosine triphosphate (ATP) biosynthesis abolishes virulence in *Cryptococcus neoformans*. *ACS Infect. Dis.* **2**, 651–663
15. Chitty, J. L., Blake, K. L., Blundell, R. D., Koh, Y., Thompson, M., Robertson, A. A. B., Butler, M. S., Cooper, M. A., Kappler, U., Williams, S. J., Kobe, B., and Fraser, J. A. (2017) *Cryptococcus neoformans* ADS lyase is an enzyme essential for virulence whose crystal structure reveals features exploitable in antifungal drug design. *J. Biol. Chem.* **292**, 11829–11839
16. Messenger, L. J., and Zalkin, H. (1979) Glutamine phosphoribosylpyrophosphate amidotransferase from *Escherichia coli*. Purification and properties. *J. Biol. Chem.* **254**, 3382
17. Wang, W., Kappock, T. J., Stubbe, J., and Ealick, S. E. (1998) X-ray crystal structure of glycinamide ribonucleotide synthetase from *Escherichia coli*. *Biochemistry* **37**, 15647–15662
18. Almassy, R. J., Janson, C. A., Kan, C.-C., and Hostomska, Z. (1992) Structures of Apo and complexed *Escherichia coli* glycinamide ribonucleotide transformylase. *Proc. Natl. Acad. Sci. U. S. A.* **89**, 6114–6118
19. Anand, R., Hoskins, A. A., Stubbe, J., and Ealick, S. E. (2004) Domain organization of *Salmonella typhimurium* formylglycinamide ribonucleotide amidotransferase revealed by X-ray crystallography. *Biochemistry* **43**, 10328–10342
20. Schrimsher, J. L., Schendel, F. J., Stubbe, J., and Smith, J. M. (1986) Purification and characterization of aminoimidazole ribonucleotide synthetase from *Escherichia coli*. *Biochemistry* **25**, 4366–4371
21. Chua, S. M. H., and Fraser, J. A. (2020) Surveying purine biosynthesis across the domains of life unveils promising drug targets in pathogens. *Immunol. Cell Biol.* **98**, 819–831
22. Sampei, G., Baba, S., Kanagawa, M., Yanai, H., Ishii, T., Kawai, H., Fukai, Y., Ebihara, A., Nakagawa, N., and Kawai, G. (2010) Crystal structures of glycinamide ribonucleotide synthetase, PurD, from thermophilic eubacteria. *J. Biochem.* **148**, 429–438
23. Li, C., Kappock, T. J., Stubbe, J., Weaver, T. M., and Ealick, S. E. (1999) X-ray crystal structure of aminoimidazole ribonucleotide synthetase (PurM), from the *Escherichia coli* purine biosynthetic pathway at 2.5 Å resolution. *Structure* **7**, 1155–1166
24. Welin, M., Grossmann, J. G., Flodin, S., Nyman, T., Stenmark, P., Trésaugues, L., Kotenyova, T., Johansson, I., Nordlund, P., and Lehtiö, L. (2010) Structural studies of tri-functional human GART. *Nucleic Acids Res.* **38**, 7308–7319
25. Kanagawa, M., Baba, S., Watanabe, Y., Nakagawa, N., Ebihara, A., Kuramitsu, S., Yokoyama, S., Sampei, G. I., and Kawai, G. (2016) Crystal

structures and ligand binding of PurM proteins from *Thermus thermophilus* and *Geobacillus kaustophilus*. *J. Biochem.* **159**, 313–321
26. Arras, S. D., Chitty, J. L., Blake, K. L., Schulz, B. L., and Fraser, J. A. (2015) A genomic safe haven for mutant complementation in *Cryptococcus neoformans*. *PLoS One* **10**, e0122916
27. Burdett, T. C., Desjardins, C. A., Logan, R., McFarland, N. R., Chen, X., and Schwarzschild, M. A. (2013) Efficient determination of purine metabolites in brain tissue and serum by high-performance liquid chromatography with electrochemical and UV detection. *Biomed. Chromatogr.* **27**, 122–129
28. Schendel, F. J., Cheng, Y. S., Otvos, J. D., Wehrli, S., and Stubbe, J. (1988) Characterization and chemical properties of phosphoribosylamine, an unstable intermediate in the *de novo* purine biosynthetic pathway. *Biochemistry* **27**, 2614–2623
29. Fawaz, M. V., Topper, M. E., and Firestine, S. M. (2011) The ATP-grasp enzymes. *Bioorg. Chem.* **39**, 185–191
30. Thoden, J. B., Kappock, T. J., Stubbe, J., and Holden, H. M. (1999) Three-dimensional structure of N5-carboxyaminoimidazole ribonucleotide synthetase: A member of the ATP grasp protein superfamily. *Biochemistry* **38**, 15480–15492
31. Thoden, J. B., Firestine, S., Nixon, A., Benkovic, S. J., and Holden, H. M. (2000) Molecular structure of *Escherichia coli* PurT-encoded glycinamide ribonucleotide transformylase. *Biochemistry* **39**, 8791–8802
32. Zhang, Y., White, R. H., and Ealick, S. E. (2008) Crystal structure and function of 5-formaminoimidazole-4-carboxamide ribonucleotide synthetase from *Methanocaldococcus jannaschii*. *Biochemistry* **47**, 205–217
33. Holm, L. (2020) DALI and the persistence of protein shape. *Protein Sci.* **29**, 128–140
34. Krissinel, E., and Henrick, K. (2007) Inference of macromolecular assemblies from crystalline state. *J. Mol. Biol.* **372**, 774–797
35. Janbon, G., Ormerod, K. L., Paulet, D., Byrnes, E. J., 3rd, Yadav, V., Chatterjee, G., Mullapudi, N., Hon, C. C., Billmyre, R. B., Brunel, F., Bahn, Y. S., Chen, W., Chen, Y., Chow, E. W., Coppée, J. Y., *et al.* (2014) Analysis of the genome and transcriptome of *Cryptococcus neoformans* var. grubii reveals complex RNA expression and microevolution leading to virulence attenuation. *PLoS Genet.* **10**, e1004261
36. Fraser, J. A., Subaran, R. L., Nichols, C. B., and Heitman, J. (2003) Recapitulation of the sexual cycle of the primary fungal pathogen *Cryptococcus neoformans* var. gattii: Implications for an outbreak on Vancouver Island, Canada. *Eukaryot. Cell* **2**, 1036–1045
37. Goins, C. L., Gerik, K. J., and Lodge, J. K. (2006) Improvements to gene deletion in the fungal pathogen *Cryptococcus neoformans*: Absence of Ku proteins increases homologous recombination, and co-transformation of independent DNA molecules allows rapid complementation of deletion phenotypes. *Fungal Genet. Biol.* **43**, 531–544
38. Arras, S. D., and Fraser, J. A. (2016) Chemical inhibitors of non-homologous end joining Increase targeted construct integration in *Cryptococcus neoformans*. *PLoS One* **11**, e0163049
39. Pitkin, J. W., Panaccione, D. G., and Walton, J. D. (1996) A putative cyclic peptide efflux pump encoded by the TOXA gene of the plant-pathogenic fungus *Cochliobolus carbonum*. *Microbiology (Reading)* **142**, 1557–1565
40. Southern, E. M. (1975) Detection of specific sequences among DNA fragments separated by gel electrophoresis. *J. Mol. Biol.* **98**, 503–517
41. Chaskes, S., and Tyndall, R. L. (1975) Pigment production by *Cryptococcus neoformans* from para- and ortho-Diphenols: Effect of the nitrogen source. *J. Clin. Microbiol.* **1**, 509–514
42. Christensen, W. B. (1946) Urea Decomposition as a means of Differentiating *Proteus* and *Paracolon* cultures from each other and from *Salmonella* and *Shigella* types. *J. Bacteriol.* **52**, 461–466
43. Price, M. F., Wilkinson, I. D., and Gentry, L. O. (1982) Plate method for detection of phospholipase activity in *Candida albicans*. *Sabouraudia* **20**, 7–14
44. Studier, F. W. (2005) Protein production by auto-induction in high-density shaking cultures. *Protein Expr. Purif.* **41**, 207–234
45. Sonn-Segev, A., Belacic, K., Bodrug, T., Young, G., VanderLinden, R. T., Schulman, B. A., Schimpf, J., Friedrich, T., Dip, P. V., Schwartz, T. U., Bauer, B., Peters, J.-M., Struwe, W. B., Benesch, J. L. P., Brown, N. G., *et al.* (2020) Quantifying the heterogeneity of macromolecular machines by mass photometry. *Nat. Commun.* **11**, 1772
46. Cheng, Y. S., Rudolph, J., Stern, M., Stubbe, J., Flannigan, K. A., and Smith, J. M. (1990) Glycinamide ribonucleotide synthetase from *Escherichia coli*: Cloning, overproduction, sequencing, isolation, and characterization. *Biochemistry* **29**, 218–227
47. McPhillips, T. M., McPhillips, S. E., Chiu, H. J., Cohen, A. E., Deacon, A. M., Ellis, P. J., Garman, E., Gonzalez, A., Sauter, N. K., Phizackerley, R. P., Soltis, S. M., and Kuhn, P. (2002) Blu-ice and the Distributed Control system: Software for data acquisition and instrument control at macromolecular crystallography beamlines. *J. Synchrotron Radiat.* **9**, 401–406
48. Kabsch, W. (2010) XDS. *Acta Crystallogr. D Biol. Crystallogr.* **66**, 125–132
49. Winn, M. D. (2003) An overview of the CCP4 project in protein crystallography: An example of a collaborative project. *J. Synchrotron Radiat.* **10**, 23–25
50. McCoy, A. J., Grosse-Kunstleve, R. W., Adams, P. D., Winn, M. D., Storoni, L. C., and Read, R. J. (2007) Phaser crystallographic software. *J. Appl. Crystallogr.* **40**, 658–674
51. Adams, P. D., Afonine, P. V., Bunkóczi, G., Chen, V. B., Davis, I. W., Echols, N., Headd, J. J., Hung, L. W., Kapral, G. J., Grosse-Kunstleve, R. W., McCoy, A. J., Moriarty, N. W., Oeffner, R., Read, R. J., Richardson, D. C., *et al.* (2010) PHENIX: A comprehensive Python-based system for macromolecular structure solution. *Acta Crystallogr. D Biol. Crystallogr.* **66**, 213–221
52. Emsley, P., and Cowtan, K. (2004) Coot: Model-building tools for molecular graphics. *Acta Crystallogr. D Biol. Crystallogr.* **60**, 2126–2132
53. Schlee, S., Straub, K., Schwab, T., Kinateder, T., Merkl, R., and Sterner, R. (2019) Prediction of quaternary structure by analysis of hot spot residues in protein-protein interfaces: The case of anthranilate phosphoribosyltransferases. *Proteins* **87**, 815–825
54. Daubner, S. C., Young, M., Sammons, R. D., Courtney, L. F., and Benkovic, S. J. (1986) Structural and mechanistic studies on the HeLa and chicken liver proteins that catalyze glycinamide ribonucleotide synthesis and formylation and aminoimidazole ribonucleotide synthesis. *Biochemistry* **25**, 2951–2957
55. Antle, V. D., Liu, D., McKellar, B. R., Caperelli, C. A., Hua, M., and Vince, R. (1996) Substrate specificity of glycinamide ribonucleotide synthetase from chicken liver. *J. Biol. Chem.* **271**, 8192–8195
56. Nierlich, D. P. (1978) Phosphoribosylglycinamide synthetase from *Aerobacter aerogenes*. *Methods Enzymol.* **51**, 179–185
57. Bera, A. K., Chen, S., Smith, J. L., and Zalkin, H. (2000) Temperature-dependent function of the glutamine phosphoribosylpyrophosphate amidotransferase ammonia channel and coupling with glycinamide ribonucleotide synthetase in a hyperthermophile. *J. Bacteriol.* **182**, 3734–3739
58. Arras, S. D. M., Ormerod, K. L., Erpf, P. E., Espinosa, M. I., Carpenter, A. C., Blundell, R. D., Stowasser, S. R., Schulz, B. L., Tanurdzic, M., and Fraser, J. A. (2017) Convergent microevolution of *Cryptococcus neoformans* hypervirulence in the laboratory and the clinic. *Sci. Rep.* **7**, 17918